Effects of snow redistribution parameterization on simulated snow thickness validated by MOSAiC observations

Fengguan Gu[1] Changwei Liu[1] Bo Han[1] Qinghua Yang[1] Jiping Liu[1*]

1. School of Atmospheric Sciences, Sun Yat-sen University, and Southern Marine Science and Engineering Guangdong Laboratory (Zhuhai), Zhuhai, China

Corresponding authors: Jiping Liu (liujp63@mail.sysu.edu.cn)

Abstract

Snow plays a critical role in the mass and energy balance of sea ice through its insulating properties and high albedo. Based on observations from the Multidisciplinary Drifting Observatory for the Study of Arctic Climate (MOSAiC) campaign, we assess the influence of two Icepack snow redistribution parameterizations, bulk redistribution and blowing snow redistribution, on snow thickness simulations using the Icepack column model. Our results show that, without snow redistribution, snow thickness is overestimated in winter and spring. The bulk redistribution scheme slightly reduces snow accumulation, while the blowing snow scheme further increases agreement with observations but still overestimates snow accumulation during major snowfall events. Sensitivity experiments indicate that setting P=4, corresponding to a ridged-to-level snow mass ratio of 5, in the bulk redistribution scheme yields the best agreement with snow observations (mean absolute error (MAE) reduced by approximately 73% relative to the baseline bulk experiment). In the blowing snow scheme, the snow erosion coefficient is treated as an effective tuning parameter. When observed sea ice concentration is prescribed, setting the snow erosion coefficient to 2.4×10^{-5} produces simulated accumulated snow loss to leads consistent with observations and improves

Deleted: snow redistribution

Deleted: (snwITDrdg)

Deleted: shows biases during snowfall events

Deleted: Sensitivity experiments indicate that setting the ratio of snow mass on ridges to that on level ice to 4 in the bulk scheme yields the best agreement with snow observations (MAE = 6.2 mm)

Deleted: snwITDrdg

the simulated snow thickness (MAE reduced by approximately 51% relative to the original blowing snow experiment). This study provides new insights into snow thickness simulation and the parameterization of snow redistribution, offering valuable guidance for improving modeling of snow thickness on Arctic sea ice.

1. Introduction

Snow cover on sea ice exerts a critical influence on the mass and energy balance of the ice through its high albedo and strong insulating properties (Callaghan et al., 2011; Maykut & Untersteiner, 1971; Webster et al., 2018). Its impact, however, is multifaceted and seasonally variable. In winter, snow insulates sea ice from the atmosphere, suppressing ice growth. In summer, the presence of snow generally increases surface albedo and can delay the onset of surface melt; once melting begins, snowmelt can contribute to meltwater production and melt-pond formation, enhancing solar energy absorption (Eicken et al., 2004; Perovich et al., 2002; Polashenski et al., 2012). Snow accumulation can also lead to flooding and the formation of snow-ice, a process well documented on Antarctic first-year ice (Jeffries et al., 2001; Leppäranta, 1983; Maksym & Jeffries, 2000; Massom et al., 2001), and occasionally observed in the Arctic with the ongoing thinning of sea ice (Kwok, 2018; Granskog et al., 2017; Merkouriadi et al., 2017, 2020). Additionally, summer snow meltwater can percolate into the snowpack and refreeze as superimposed ice, further contributing to sea ice mass (Cheng et al., 2003; Eicken et al., 2004; Wang et al., 2015). Therefore, an accurate representation of snow thickness is essential for improving sea ice modeling and evolution.

The spatial distribution of snow thickness on sea ice is primarily controlled by snowfall (Wagner et al., 2022), but it is also strongly shaped by wind-driven snow redistribution. Strong winds can lift snow particles from the surface, and a portion of these suspended

Deleted: MAE = 6.4 mm

Deleted: Arctic snow thickness modeling

Deleted: thick snow preserves high albedo and resists melting, while thin snow is more prone to forming melt ponds, enhancing solar energy absorption

Deleted: in

Deleted: ,

Deleted: increasingly reported

Deleted: In snow thickness simulations, snowfall is the primary factor influencing the spatial distribution of snow thickness (Wagner et al., 2022). In addition, snow redistribution parameterizations also influence the simulated snow thickness. The Icepack 1.3.2 sea ice column model includes two snow redistribution processes: bulk redistribution and snwITDrdg redistribution. The bulk snow redistribution parameterization is based on previous observational studies (Sturm et al., 2002) and assumes that approximately 30% of snowfall is effectively lost due to ice surface heterogeneity, such as leads and ridges. This approach reduces the effective snowfall reaching the ice surface, thereby decreasing the simulated snow thickness (Hunke et al., 2022). Beyond bulk redistribution, snwITDrdg redistribution is a crucial physical process that determines the spatial distribution of snow thickness (Olivier Lecomte et al., 2015; Leonard & Maksym, 2011; Liston et al., 2020). In snwITDrdg redistribution,

Deleted: s

particles fall into open leads (Olivier Lecomte et al., 2015; Leonard & Maksym, 2011; Petty et al., 2018), while the remaining particles are redistributed on the snow surface, thereby altering the spatial distribution of snow thickness and affecting the mass and energy balance of the snow (Luo & Zhang, 2022). Blowing snow can also facilitate the sublimation of suspended snow particles (Déry & Yau, 2002; Liston et al., 2020), and studies have shown that under the same atmospheric conditions, the sublimation rate of blowing snow is two orders of magnitude higher than that of a stationary snow surface (Schmidt, 1982). Previous modeling studies have shown that wind-driven redistribution and blowing-snow processes can substantially modify the snow mass budget on polar sea ice through snow transport, sublimation, and redistribution among different ice surface types (Déry and Tremblay, 2004; Chung et al., 2011; Lecomte et al., 2015). Recent satellite-based studies during MOSAiC further indicate that blowing snow was active over Arctic sea ice and may represent an important sink in the snow-on-sea-ice budget (Robinson et al., 2025, 2026)

Observational studies highlight the importance of these processes for the snow mass budget. In the Southern Ocean, Leonard and Maksym (2011) suggested that approximately half of the precipitation over sea ice could be lost to leads under the observed conditions. During the MOSAiC expedition, observations indicate that under typical winter conditions, leads have a minimal impact on the snow mass balance, but when snowfall occurs alongside strong winds and high temperatures, 65%-100% of the recent snowfall can fall into open leads (Clemens Sewall et al., 2023), as strong winds promote snow redistribution and higher temperatures prevent rapid lead refreezing. Recent work has also emphasized that snow sinks on level sea ice can vary strongly with atmospheric forcing, surface state, and ice conditions (Merkouriadi et al., 2025) Parameterizations of snow redistribution by wind have been applied in climate models (Olivier Lecomte et al., 2015) and reanalysis-forced reconstruction models of snow evolution on sea ice, such as NESOSIM (Petty et al., 2018). However, these approaches typically rely on simplified assumptions or tuning parameters and have not been

Deleted: ; Van den Broeke et al., 2004

Deleted: about half of the snowfall eventually falls into open leads (Leonard & Maksym, 2011)

Deleted: data assimilation products

extensively evaluated against detailed observations.

In Icepack 1.3.2, the empirical coefficients in the snow redistribution parameterization remain uncertain and have not been systematically constrained using recent MOSAiC observations. Although newer versions of Icepack have since been released, we used Icepack 1.3.2 to maintain consistency with the model configuration used in this study and focused on evaluating the snow redistribution parameterizations implemented in that version. Previous studies using the Icepack model have examined the performance of snow redistribution processes in simulating snow thickness (Hao et al., 2025; Zhao et al., 2025). In particular, Zhao et al. (2025) evaluated snow evolution along the MOSAiC drift trajectory using Icepack configurations with no redistribution, bulk redistribution, and blowing-snow redistribution, highlighting the importance of snow redistribution and melt-pond schemes for simulated sea ice thickness. However, the lack of accurate snowfall observations and measurements of snow blown into open leads introduces uncertainty in snow thickness simulations. In this study, we use atmospheric, oceanic and sea ice observations from the MOSAiC expedition to evaluate Icepack's snow redistribution, examine its impact on simulated Arctic snow thickness and explore avenues for further optimization. Section 2 describes the data and methods. Section 3 presents the performance of different snow redistribution processes on snow thickness simulation (3.1) and proposes improvements to the snow redistribution parameterization (3.2). Section 4 provides conclusions and discussions.

Deleted: The Icepack 1.3.2 sea ice column model incorporates a parameterization for snow redistribution (Lecomte et al., 2013), yet many of its empirical coefficients have not been updated with recent observations or systematically validated.

2. Data and methods

2.1 Icepack

The Icepack single-column model is a state-of-the-art numerical model managed by the CICE consortium. It contains physical processes that affect sea ice thickness within a single grid cell without reference to adjacent grid cells. Subgrid ice classes are described by dividing the ice area fraction into discrete thickness categories within the single

Icepack colum. The model solves a set of equations that represent ice dynamics, thermodynamics, and mechanical redistribution (ridging). In this single-column configuration, lateral interactions with adjacent grid cells are not represented; changes in the ridged-ice fraction are handled through the prescribed ice thickness distribution and the mechanical redistribution scheme within the column. This study used Icepack version 1.3.2 (Hunke et al., 2022). The focus is on the effects of snow redistribution parameterization on snow thickness simulation. The Icepack simulation was conducted December 2019 to July 2020. The key model settings and physical parameterizations are summarized in Table 1 (Gu et al., 2022). In this single-column Icepack configuration, ocean temperature, salinity, and current forcing are prescribed from observations and used as external forcing for the ice column. Snow deposited into leads is treated as an immediate snow mass flux from the ice-snow column to the ocean; however, the resulting freshwater input is not allowed to feed back onto ocean salinity, ocean stratification, or ocean-to-ice heat fluxes. Following Clemens-Sewall et al. (2022), the Icepack ice thickness distribution is divided into 15 categories to more accurately represent the distribution of snow thickness.

Table 1. Detailed options of physical parameterizations and model settings for ICEPACK. SST signifies sea surface temperature.

ICEPACK	Value
Time step	3600 s
Number of layers in the ice	7
Number of layers in the snow	1
Ice thickness categories	15 (Clemens-Sewall et al., 2022)
Initial ice thickness	105 cm (mean observe)
Initial snow depth	17 cm (mean observe)
Ice thermodynamic	Mushy layer (Turner et al., 2013)

Deleted: within each grid cell

Deleted: The observed atmospheric and oceanic forcing data are used as input for model simulations.

Deleted: The model is initialized with observed ice thickness and snow thickness. The model settings, physical parameterizations are the same as those of previous studies (Gu et al., 20242)

Formatted: Indent: First line: 0 ch

Formatted: Font: 10.5 pt, Bold

Formatted Table

Formatted: Font: 10.5 pt

Formatted: Font: 10.5 pt

Formatted: Font: 10.5 pt

Formatted: Font: 10.5 pt

Formatted: Font: 10.5 pt

Formatted: Font: 10.5 pt

Formatted: Font: 10.5 pt

Shortwave radiation	Delta-Eddington (Briegleb and Light, 2007)	Formatted: Font: 10.5 pt
Melt ponds (superimposed ice)	Not used in this study	Formatted: Font: 10.5 pt
Ocean heat transfer coefficient	0.006 (Maykut and McPhee, 1995)	Formatted: Font: 10.5 pt
SST restoring timescale (days)	0 (use observed SST as oceanic forcing)	Formatted: Font: 10.5 pt
Ocean friction velocity minimum (m s^{-1})	0.0005 (Tsamados et al., 2013)	Formatted: Font: 10.5 pt

2.2 Observational data

For this study, we used a comprehensive set of observational data encompassing atmospheric, oceanic, sea ice and snow thickness measurements collected during the MOSAiC expedition, which took place from October 2019 to September 2020. All observations were obtained within an area of approximately 15 km (Bliss et al., 2023). The atmospheric data included the Met City monitoring station and three Atmospheric Surface Flux Stations (Shupe et al., 2022). We used averaged atmospheric data from Met City and three ASFS sites as forcing for Icepack. The variables include downward shortwave and longwave radiation, 2 m air temperature, 2 m specific humidity, and 10 m wind speed. The ASFS 2 m wind speed was extrapolated to 10 m using a power-law relationship with a sea-ice surface roughness length of 1.0×10^{-3} m, following the ECMWF-IFS model (Ruti et al., 2008).

Oceanographic data comprised 10-meter sea temperature and salinity measurements from eight Conductivity, Temperature, and Depth (CTD) buoys, as well as 3-meter sea temperature, salinity, and current velocity data from four autonomous ocean flux buoys. Because all ocean temperature and salinity observations were located within the mixed layer depth (Rabe et al., 2022), the 10-m and 3-m measurements were combined to obtain mixed-layer representative time series and then spatially averaged across the buoys. These time-dependent temperature and salinity series were prescribed as external ocean forcing in the Icepack simulations. The observed relative velocities

between sea ice and the ocean surface current from the four autonomous ocean flux buoys were used to calculate the friction velocity, which was then used to estimate ocean–ice heat exchange. Although Icepack prescribes friction velocity as a fixed constant by default, we implemented a quadratic drag law following Jenkins et al. (2010), $u_*^2 = c_w U^2$, where c_w is the dimensionless ice–ocean drag coefficient and U is the ice velocity relative to the ocean surface current.

The ice opening and closing rates (s^{-1}) are derived from SAR-based sea ice divergence in the Transpolar Drift during MOSAiC 2019/2020 (von Albedyll, 2024), following the method described by Bitz (n.d.). In addition, precipitation data from the present weather detector (PWD) on the deck of the Polarstern and from the ERA5 reanalysis (Wagner et al., 2022) were used. Precipitation forcing is an important source of uncertainty in the snow-thickness simulations. Following Wagner et al. (2022), we used the average of precipitation from the PWD and ERA5 reanalysis as the model precipitation forcing, because MOSAiC precipitation estimates differ substantially among products and the actual precipitation likely lies between the PWD and ERA5 estimates. The resulting cumulative precipitation from 31 October 2019 to 26 April 2020 is 91 mm, within the observationally constrained range reported by Wagner et al. (2022). Nevertheless, uncertainties in precipitation timing, frequency, and magnitude may contribute to biases in simulated snow accumulation, especially during individual snowfall events.

The Icepack was initialized using MOSAiC observations of initial snow thickness and ice thickness from the Snow and Ice Mass Balance (SIMBA) array (Lei et al., 2022). In this study, seven buoys were selected according to their operational periods (Table 2), and their mean snow thickness and mean ice thickness were used to evaluate the simulated snow and ice thickness. According to the site descriptions summarized by Perovich et al. (2023), these buoys were deployed over both first-year ice and second-year ice. Because the Icepack simulations used a fixed snow density of 330 kg m^{-3}, whereas the observed snow density varied from approximately 200 to 400 kg m^{-3}, a

Deleted: The observed current velocities from the four autonomous ocean flux buoys were used to calculate the friction velocity, which was used to estimate ocean – ice heat exchange.

Deleted: The observed sea temperature, salinity were prescribed as time-dependent external forcing in the Icepack simulations. The observed current velocities were used to calculate the friction velocity, which is used to estimate ocean–ice heat exchange. All ocean observations are confined within the mixed layer depth (Rabe et al., 2022). The spatially averaged values of these observations are used as oceanic forcing to simulate snow thickness.

Deleted: Following Wagner et al. (2022), who reported that the actual precipitation during MOSAiC lies between the PWD and ERA5 estimates, we use the average of these two datasets as the precipitation forcing, which is consistent with the observed range reported in their study. This yields a cumulative total of 91 mm from 31 October 2019 to 26 April 2020, within the observed range of 72 to 107 mm.

Deleted: Observed snow thickness was obtained from

Deleted: 1

Deleted: (FYI)

Deleted: (SYI)In this study, 7 buoys were selected based on their operational periods, and their mean snow thickness and mean ice thickness were used to evaluate the simulated snow and ice thickness

Formatted: Font: (Asian) Songti SC, 12 pt, Font color: Auto

Formatted: Font: (Asian) Songti SC, 12 pt, Font color: Auto

direct comparison based only on snow depth would not account for variations in snow mass. Therefore, the observed snow thickness were converted to snow water equivalent (SWE) using fitted SnowMicroPen (SMP) density–SWE relationships (Wagner et al., 2022) , allowing the observations and simulations to be compared in terms of snow mass. Although this empirical conversion may introduce additional uncertainty, it provides a more physically consistent basis for evaluating the simulated snow mass. Daily sea ice concentration data were obtained from the Advanced Microwave Scanning Radiometer 2 (AMSR2) using the Arctic Sea Ice (ASI) algorithm (Spreen et al., 2008) developed at the University of Bremen, at a spatial resolution of 3.125 km.

Table 2. Characteristics of the seven MOSAiC Snow and Ice Mass Balance Array (SIMBA) buoys used in this study, including deployment site, sea-ice type, observation period, and initial snow and ice conditions. The selected buoys were deployed over both first-year ice (FYI) and second-year ice (SYI) during the MOSAiC expedition (Perovich et al., 2023; Salganik et al., 2023). CO refers to the Central Observatory, L1-L3 are Local Scale Distributed Network sites located within a few kilometers of the Central Observatory, and M6 is a Mesoscale Distributed Network site located tens of kilometers from the Central Observatory.

Buoy ID	Site	Ice Type	Start Date	End Date	Initial Ice Thickness (m)	Initial snow Thickness (m)
2019T56	CO	SYI	2019-11-02	2020-07-03	0.42	0.18
2019T62	CO	SYI	2019-10-30	2020-07-05	0.80	0.20
2019T63	L2	SYI	2019-11-25	2020-07-27	1.08	0.12
2019T64	M6	SYI	2019-11-27	2020-08-01	1.70	0.16
2019T66	CO	FYI	2019-10-30	2020-08-02	0.42	0.10
2019T67	L1	SYI	2019-11-09	2020-07-07	1.36	0.22
2019T70	L3	FYI	2019-10-10	2020-07-11	0.48	0.06

Deleted: Snow observations

Formatted: Font: (Default) Times New Roman, (Asian) Songti SC, 12 pt, Not Bold, Font color: Auto

Deleted: 1

Formatted: Font: (Default) Times New Roman, (Asian) Songti SC, 12 pt, Not Bold, Font color: Auto

Formatted: Space Before: 16.3 pt, After: 0 pt

Formatted: Font: (Default) Times New Roman, Not Bold

Formatted: Font color: Auto

Formatted: Font color: Auto

Formatted: Font color: Auto

Formatted: Font color: Auto

Formatted: Font color: Auto

Formatted: Font color: Auto

Formatted: Font color: Auto

Formatted: Font color: Auto

2.3 Snow redistribution physical process

In Icepack, snow mass evolves through snowfall, condensation, melting, sublimation, snow-ice formation, and wind-driven processes (Hunke et al., 2022). Icepack includes two snow redistribution processes: bulk redistribution and snwITDrdg redistribution. In the bulk redistribution scheme, the parameterization is motivated by SHEBA observations showing that snow in the vicinity of ice ridges was approximately 30% greater than that on level ice (Sturm et al., 2002). This observed contrast may result from several physical processes, including wind-driven redistribution of snow from level ice toward ridged areas, snow loss into leads, sublimation, and snow incorporation during ridging. In Icepack, these unresolved processes are represented in a simplified way by assuming that a fraction of incoming snowfall over level ice is instantaneously diverted into the ocean through leads, thereby reducing the effective snowfall contributing to snow accumulation on level ice (Hunke et al., 2022). Mathematically, the amount of snow entering the leads is given by:

$$s_f' = s_f \left[a_{lvl} \left(\frac{p}{1+p} \right) \right] \quad (1)$$

where s_f is the snowfall rate, a_{lvl} is the area of the level ice within a grid cell, and $1+p$ represents the ratio of snow mass on ridged ice to that on level ice, while p represents the excess snow mass on ridged ice relative to level ice.

In the processes of snwITDrdg redistribution, the erosion rate of the snow is expressed as:

$$\Phi_{local}^{T} = \left(\frac{\partial m}{\partial t} \right)_{erosion} = -\frac{\gamma}{\sigma ITD} (V - V^*) \frac{\rho_{max} - \rho_s}{\rho_{max}} \quad (2)$$

where ρ_{max} and ρ_s are the maximum snow density and the effective snow density in Icepack, respectively. The value of ρ_{max} is set to 400 kg m^{-3} (Macfarlane et al., 2023). When erosion begins, snow particles start to suspend when the instantaneous wind

Deleted: Snow acts as an insulating layer between the atmosphere and sea ice, altering the albedo of the sea ice surface, thereby exerting a strong influence on the simulated sea ice mass and energy balance.

Deleted: ¶

Deleted: based on SHEBA observational data, Icepack assumes that snow thickness in proximity of ice ridges is approximately 30% greater than that on level ice. To account for this preferential accumulation on ridges, Icepack effectively reduces the fraction of snowfall contributing to snow accumulation on level ice, which leads to a decrease in the simulated snow thickness over these areas (Hunke et al., 2022). The reduced snowfall represents snow that is instantaneously redistributed and lost to the ocean through leads.…

Deleted: layer

Deleted: p is the ratio of snow depth on ridges to that on layer ice.

Deleted: After

speed V exceeds a threshold (V^*). σITD is the standard deviation of the sea ice thickness distribution within a grid cell (Hunke et al., 2022). γ is a tuning coefficient that modulates the snow erosion rate, set to 1×10^{-5} kg m^{-2} (Lecomte et al., 2015). In Icepack, the default/background snow density is 330 kg m^{-3}, but the snwITDrdg scheme can also account for wind-induced compaction of the upper snow layer into denser wind slabs. The threshold V^* is calculated from the effective snow density following Lecomte et al. (2013), using $\rho_s = 174 + 44.6V^*$. Therefore, when $\rho_s = 330$ kg m^{-3}, V^* is approximately 3.5 m s^{-1}. This V^* represents the wind speed associated with compacting snow to the effective density used in the parameterization. Further details are provided in the Icepack technical documentation (Hunke et al., 2022).

The remaining suspended snow particles are redistributed over the ice surface as:

$$\Phi^R_{local}\Delta t = a_i(1-f)\Phi^T_{local}\Delta t \quad (3)$$

Where f represents the fraction of suspended snow particles lost within the leads (Lecomte et al., 2013):

$$f = (1-a_i)\exp\left(\frac{-\sigma_{ITD}}{\sigma_{ref}}\right) \quad (4)$$

Where σ_{ref} =_1 m, and a_i is the area of the ice within a grid cell. Here σ_{ref} is a reference scale for the standard deviation of the ice thickness distribution. The exponential term indicates that snow loss to leads decreases as σ_{ITD} increases. Physically, a larger σ_{ITD} reflects more ridged or deformed ice, which can shelter drifting snow and promote snow accumulation near ridges, thereby reducing the fraction of suspended snow transported into leads. The remaining suspended snow is redistributed locally among the ice thickness categories, preferentially increasing snow accumulation over ridged/deformed ice while reducing snow over more exposed level ice.

Formatted: Superscript

Deleted: In Icepack, the default snow density is set to 330 kg/m^3 The threshold wind speed for snow erosion is calculated based on this snow density following Lecomte et al. (2013). Icepack further accounts for wind-induced compaction of the upper snow layer into denser wind slabs, which limits subsequent snow erosion; details are provided in the Icepack technical documentation.

Deleted: σITD

Deleted: σref

Formatted: Font: (Intl) Times New Roman

In addition to the redistribution mechanisms described above, the snwITDrdg scheme relies on several simplifying assumptions that influence the representation of blowing-snow processes in Icepack. Snow loss to leads therefore occurs both through direct snowfall onto open water when sea ice concentration is below unity and through wind-driven snow erosion when wind speed exceeds a threshold. Icepack assumes local conservation of snow mass during blowing-snow redistribution, neglecting non-local transport between grid cells (Lecomte et al., 2015). Snow redistribution directly modifies the snow thickness associated with each ice thickness category and therefore affects the thermodynamic evolution of snow and ice. However, because Icepack assumes a uniform snow thickness within each category, subgrid-scale spatial heterogeneity in snow redistribution is not explicitly resolved. The uniform snow-thickness assumption applies to the thermodynamic calculation within each ice thickness category, whereas the redistribution and radiation calculations account for the effects of level and ridged ice fractions. Although snow thickness directly affects the thermodynamic mass balance, the effects of its spatial variability are primarily represented through the surface radiation scheme, which responds to changes in effective surface fractions (Hunke et al., 2022).

Deleted:

3. Results

3.1 Snow Thickness Simulation Based on Different Snow Redistribution Processes

To simulate snow thickness during the MOSAiC period, we force the Icepack sea ice column model with mean atmospheric and oceanic observations. We assess the impact of the snow redistribution parameterization by comparing three Icepack configurations: no-redistribution experiment, bulk redistribution (bulk), and blowing-snow redistribution (snwITDrdg). All snow thickness values are converted to SWE for consistency with observations. Figure 1d shows that observed SWE increased from ~55

Deleted: no redistribution (none)

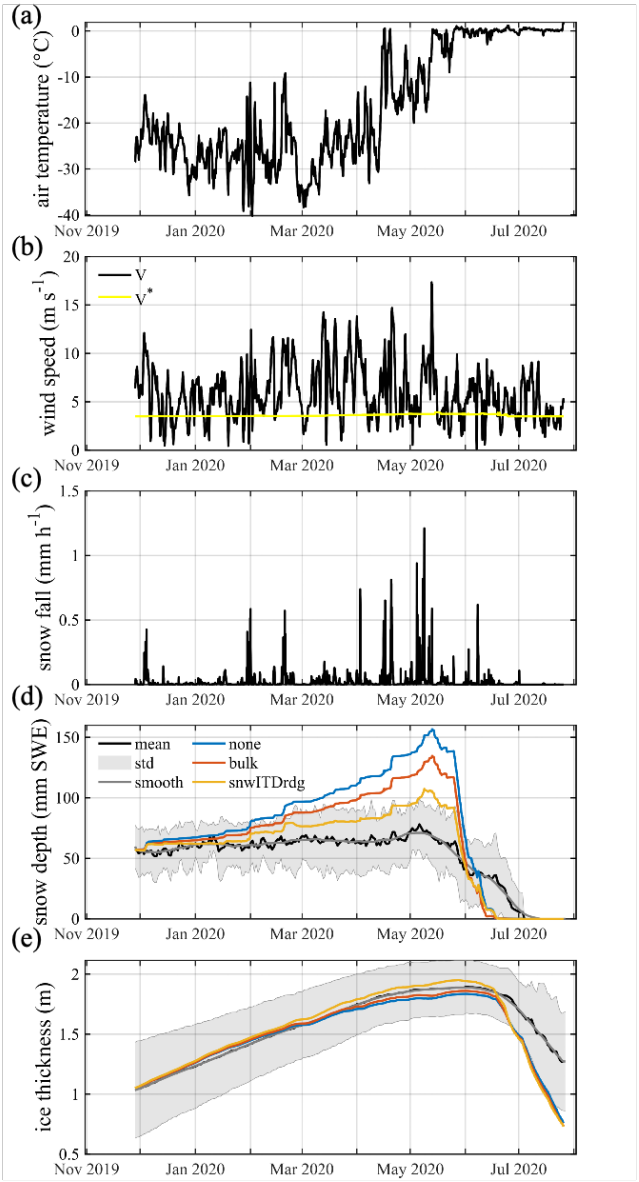
Deleted: snow water equivalent

Deleted: snow

mm in December 2019 to ~65 mm by March 2020, then slightly decreased in April, peaked at 75 mm in May, and rapidly melted as temperatures rose (Figure 1a), with complete melt by July. The observed ice thickness increased from about 1.0 m in December 2019 to a maximum of about 1.9 m in early June, followed by rapid summer melt, decreasing to ~1.3 m by the end of July (Figure 1e).

Deleted: 0

Deleted: Given the critical role of precipitation in snow accumulation, we follow Wagner et al. (2022), who reported that actual precipitation lies between PWD and ERA5 estimates. We use the average of these two datasets, which is consistent with the observed range reported in their study, yielding a cumulative total of 91 mm from October 31, 2019, to April 26, 2020, within the observed range of 72–107 mm.



389

390 Figure 1. Simulation time series of (a) 2 m air temperature, (b) 10 m wind speed, (c)
391 snowfall, (d) snow thickness, and (e) ice thickness. The black line represents the
392 observation, and the yellow line in (b) represents the wind speed threshold (V^*) for

Deleted: Time series simulation

Deleted: windstar

snow erosion and suspension in the snwITDrdg scheme. In (d) and (e), the thick black line and grey shading represent the multi-site mean observations and their standard deviation, respectively, while the gray line indicates the 20d moving average of the mean observations. The blue, red, and yellow lines represent the snow thickness simulations with no redistribution, bulk redistribution, and snwITDrdg redistribution, respectively.

For the no-redistribution experiment, simulated SWE is overestimated relative to observations starting in mid-January, particularly during periods of snowfall. The simulation peaks at 155 mm on May 13, compared with the observed corresponding to an overestimation of about 80 mm SWE. It then rapidly melts, with complete melt occurring by June 17. The bulk scheme reduces snow thickness slightly, but the seasonal trend remains similar, with a peak SWE of approximately 130 mm and a mean absolute error (MAE) of approximately 23 mm SWE before June. In contrast, the snwITDrdg scheme significantly reduces SWE compared with the no-redistribution experiment and bulk scheme, lowering the peak SWE to approximately 105 mm and reducing the MAE to approximately 13 mm SWE before June. According to the parameterization described in Section 2.3, snow redistribution is activated when the wind speed exceeds the threshold for snow erosion (~3.5 m/s Figure 1b). Under these conditions, suspended snow particles are redistributed over the ice surface or deposited into open leads (Lecomte et al., 2013, 2015; Hunke et al., 2022), thereby reducing snow accumulation and bringing the simulated temporal evolution of SWE closer to the observations. However, even with blowing-snow redistribution, simulated snow thickness remains overestimated in winter and spring and melts too rapidly in summer (Figure 1d), indicating that none of the three default snow redistribution schemes fully reproduces the observed SWE evolution. This remaining bias motivates the parameter optimization of the snow redistribution parameterization presented in the following section.

Compared with the snow thickness simulations, the ice thickness simulations show better agreement with the observations before the onset of summer melt. The spread in

Deleted: thin

Deleted: black

Deleted: -

Deleted: ay

Deleted: ne

Deleted: We assess the impact of the snow redistribution parameterization by comparing three Icepack configurations: no redistribution (none), bulk redistribution (bulk), and blowing-snow redistribution (snwITDrdg). All snow thickness values are converted to snow water equivalent for consistency with observations. Figure 1d shows that observed snow SWE increased from ~55 mm in December 2019 to ~65 mm by March 2020, then slightly decreased in April, peaked at 70 mm in May, and rapidly melted as temperatures rose (Figure 1a), with complete melt by July. The observed ice thickness increased from about 1.0 m in December 2019 to a maximum of about 1.9 m in early June, followed by rapid summer melt, decreasing to ~1.3 m by the end of July (Figure 1e).¶

Deleted: none scheme

Deleted: and then rapidly melts, with complete melt occurring by June 17

Deleted: none

Deleted: s

Deleted: improving agreement with the observations.In contrast, the snwITDrdg scheme significantly reduces SWE, particularly during high-wind periods. When wind speed exceeds ~3.5 m/s (Figure 1b), snow particles are suspended and redistributed or deposited into open leads, reducing surface accumulation. Despite incorporating wind slab formation to limit snow suspension, frequent high winds drive continuous snow redistribution, improving agreement with observations.

Deleted: .

simulated ice thickness among experiments is much smaller than the spread in snow thickness. The no-redistribution and bulk redistribution experiments slightly underestimate ice thickness during April to mid-June, while the snwITDrdg experiment exhibits a modest overestimation during this period. After mid-June, all simulations tend to underestimate the observed ice thickness. This bias is likely attributable to the rapid melt of simulated snow thickness during summer, which leads to increased exposure of sea ice to the warm atmosphere (Figure 1e).

3.2 Optimization of the Snow Redistribution Parameterization

We conduct a series of parameter optimization experiments aimed at improving the performance of the bulk and snwITDrdg snow redistribution schemes. Specifically, we focus on optimizing P, which represents the excess snow mass on ridged ice relative to level ice in the bulk redistribution scheme, as well as the sea ice concentration and the tuning coefficient γ in the snwITDrdg redistribution scheme.

In the bulk redistribution scheme, p is set to 0.3 based on estimates from SHEBA observations conducted during 1997–1998, which suggest that snow thickness on ice ridges is approximately 30% greater than that on level ice. However, observations during the MOSAiC campaign indicate that large ridges accumulated nearly five times the snow depth of level ice (Itkin et al., 2023). Because this estimate does not include small ridges, which constitute a large fraction of ridged ice, it should be interpreted as an upper-end observational constraint. Therefore, to investigate the sensitivity of the model over an observationally supported range, we increased p from 0.3 to 4.0 to examine its impact on simulated snow and ice thickness. Based on Eq. (1), this range corresponds to $p/(1+p)$ values from approximately 0.23 to 0.80, so the fraction of snowfall passed to leads is $a_{lvl}\,p/(1+p)$. The mean absolute error was used to evaluate the agreement between simulated and observed SWE before June: $MAE = 1/n \sum |SWE_{sim} - SWE_{obs}|$, where n is the number of data points over the period prior

Deleted: none and bulk experiments

Deleted: Specifically, we focus on optimizing the ratio of snow mass on ridges to that on level ice (P)

Deleted: γ

Deleted: P

Deleted: two decades ago

Deleted: P

Deleted: To quantify the sensitivity of the model to this parameter, we conducted a series of sensitivity experiments in which P was increased from 0.3 to 4.0 to examine its impact on simulated snow and ice thickness.

Deleted: The mean absolute error (MAE; MAE = (1/n) ∑ |M

Deleted: HS_sim − HS_obs|)

to June. SWE_{sim} and SWE_{obs} the simulated and observed SWE, respectively. Therefore, the snow MAE is reported in mm SWE. The same MAE formulation was applied separately to ice thickness, with ice-thickness errors reported in m. The results show that increasing p leads to more snow being redistributed into open leads, thereby reducing the simulated snow thickness (Figure 2a). The minimum snow thickness MAE (~6.2 mm) is achieved when p = 4 (hereafter referred to as bulkm, Figure 3b). The simulations with model-simulated and prescribed AMSR2 sea ice concentration show similar sensitivity trends as p increases, with only small differences in accumulated snow loss and SWE MAE. These differences arise because prescribing AMSR2 sea ice concentration slightly modifies the level-ice and lead area fractions used in the bulk redistribution calculation.

Deleted: HS_sim

Deleted: HS_obs

Deleted: denote the simulated and observed snow and ice thickness, respectively, was used as the evaluation metric

Deleted: P

Deleted: P

Deleted: b

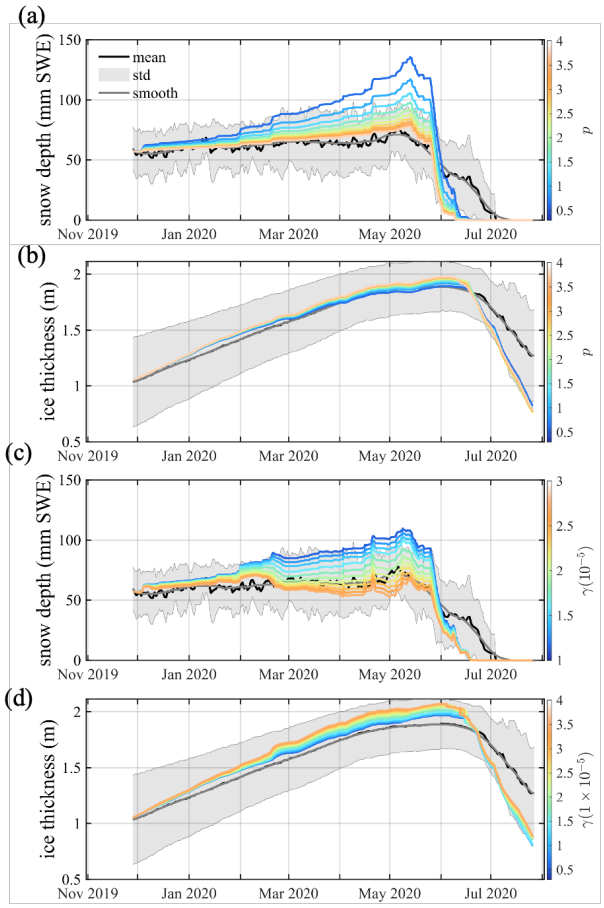


Figure 2. Time series of (a) snow thickness and (b) ice thickness from sensitivity experiments under the bulk redistribution scheme with varying P, where p is the ratio of snow depth on ridges to that on level ice, and (c) snow thickness and (d) ice thickness show the snwITDrdg sensitivity experiments with prescribed AMSR2 sea ice concentration, γ is the tuning coefficient controlling the snow erosion rate. In panels (a) and (b), the 10 colored lines represent sensitivity experiments with p ranging from 0.3 to 4.0. In panels (c) and (d), the 11 colored lines correspond to sensitivity experiments with the γ tuning coefficient ranging from 1×10^{-5} to 3×10^{-5} .

In the snwITDrdg redistribution simulation, an increase in γ represents an increase in the parameterized amount of suspended snow, while a decrease in sea ice concentration

Deleted: P

Deleted: from sensitivity experiments under the snwITDrdg scheme with varying γ

Deleted: , where

Deleted: γ

Deleted: .

Deleted: P

Deleted: γ

Deleted: γ

Deleted: enhances the number of suspended snow particles

enlarges the leads, which provide more open-water area to receive drifting snow. As a result, more snow particles are transported and deposited into these leads. There is a significant bias between the simulated and observed sea ice concentration (Figure 3a). The simulated sea ice concentration gradually decreased from 0.98 to 0.92 by the end of July, after which it decreases rapidly. The observed sea ice concentration experiences significant reductions both at the end of April and July, reaching as low as 0.7. This increases leads, thereby increasing the amount of snow blown into the leads during the snwITDrdg redistribution. We conducted 11 sensitivity experiments, varying the γ value from 1×10^{-5} to 3×10^{-5}, which increased the snow erosion rate and consequently reduced the simulated snow thickness (Figure 2c). It should be noted that γ cannot be uniquely constrained by snow depth observations alone, because its influence is strongly coupled with uncertainties in snow density (observations: 250-400 kg m^{-3}; model value: 330 kg m^{-3}) and the subgrid-scale ice thickness distribution (σ_{ITD}; observations: 0.03-0.8 m; model range: 0.4-0.8 m). Therefore, in this study, γ is interpreted as an effective parameter within the default Icepack configuration rather than as a physically universal constant.

Furthermore, using isotope-based observations from the MOSAiC expedition, Clemens-Sewall et al. (2023) found that snowfall into a lead during warmer and windier events with prolonged lead openings (19–28 April 2020) corresponded to an accumulated snow loss of approximately 7–11 mm SWE averaged over the entire surface. These observations were also used to evaluate the simulations (Figure 3b and 3c). When the snow thickness simulation is conducted without prescribing sea ice concentration, adjusting the γ coefficient does not result in accumulated snow loss to leads within the 7-11 mm range (Figure 3c). However, when the AMSR2 sea ice concentration is prescribed in the snow thickness simulation, adjusting the γ coefficient between 1.6×10^{-5} and 2.4×10^{-5} yields accumulated snow loss to leads within the 7–11 mm area-averaged SWE range. When γ is set to 2.4×10^{-5} (hereafter referred to as snwITDrdgm), the simulated snow thickness generally agrees well with the

Deleted: . γ is a tuning coefficient for the erosion rate, with a default value of 1×10^{-5}

Deleted: γ

Deleted: γ

Deleted: σITD

Deleted: γ

Deleted:

Deleted: of snow water equivalent

Deleted: per lead area

Deleted: ¶

Deleted: γ

Deleted: b

Deleted: γ

Deleted: per lead area

Deleted: γ

observations, resulting in a minimum MAE of 6.4 mm, with slight overestimations in February and May, and continued rapid melting in June compared to the observations (Figure 2c). Figure 2b and 2d show that the sensitivity of ice thickness to p and γ is smaller than the sensitivity of snow thickness, indicating that the redistribution parameters primarily affect the snowpack while exerting a weaker indirect influence on sea ice thermodynamics.

Deleted: b

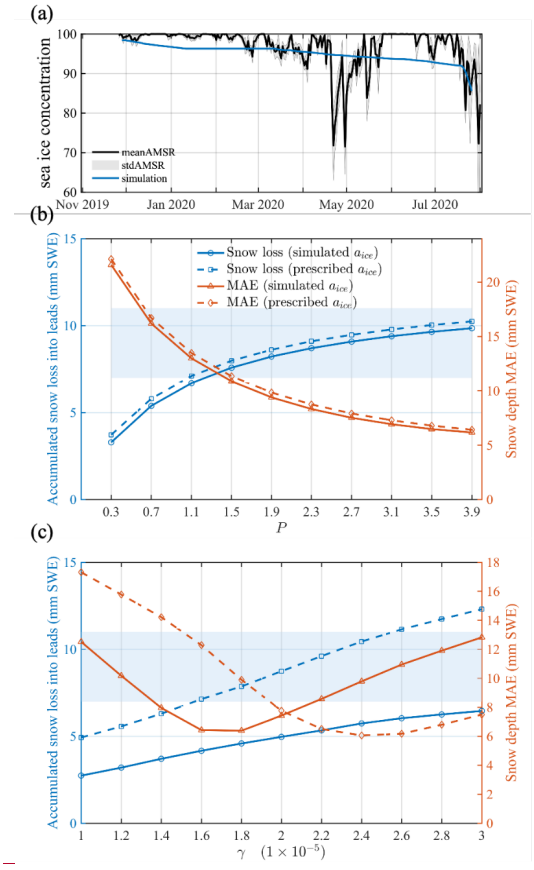


Figure 3. (a) Time series of sea ice concentration from AMSR2 observations and Icepack simulations. (b) and (c) show the statistical results for sensitivity experiments for two snow redistribution parameterizations: bulk redistribution with varying p, and

blowing-snow redistribution with varying γ, respectively. The blue line and the left blue y-axis represent the accumulated snow loss into open leads during the period from 9 April to 28 April, while the orange line and the right orange y-axis indicate the mean absolute error (MAE, in mm SWE) between simulated and observed snow thickness. The blue shaded area denotes the observed range of accumulated snow loss into open leads (~7–11 mm area-averaged SWE) based on Clemens-Sewall et al. (2023). Solid lines denote simulations with model-simulated sea ice concentration, whereas dashed lines denote simulations with prescribed observed sea ice concentration. a_{ice} denotes AMSR2 sea ice concentration

In the snow mass balance, snow thickness is influenced by snowfall (S_f), snowmelt (S_m), snow sublimation (S_{su}), snow-ice formation (S_i), and snow loss into open leads (S_{lo}). In reality, snow can also be lost during sea ice ridging when part of the snow cover becomes subducted and submerged; however, this process is not explicitly represented in the Icepack configuration used in this study. This study investigates the impact of different snow redistribution schemes, with and without prescribing sea ice concentration, on the snow mass balance. The results (Figure 4) show that, compared to the no-redistribution experiment, the bulk scheme increases the amount of snow entering the leads by reducing the snowfall reaching the ice layer. Additionally, model diagnostics indicate enhanced snow-ice formation in the snwITDrdg scheme relative to the bulk scheme. In addition to depositing a portion of snow mass into open leads, the snwITDrdg scheme diagnostically redistributes snow among ice thickness categories. This redistribution, modulated by the ridged-ice fraction and surface type within each category, results in increased snow thickness over thinner ice categories, making the ice more susceptible to surface flooding and subsequent snow-ice formation. However, enhanced snow-ice formation is not evident in the averaged SIMBA observations used in this study. Furthermore, previous studies have suggested that Icepack may overestimate snow-ice formation (Gu et al., 2022). Therefore, this category-dependent redistribution should be interpreted as a model-diagnostic mechanism rather than as a directly validated observational feature.

Compared to the bulk scheme, the bulkm configuration removes a larger fraction of

Deleted: show the statistical results for sensitivity experiments varying the γ and P parameters, respectively.

Deleted:

Deleted: per lead area

Deleted: without

Deleted: prescribed observed

Deleted: Sf

Deleted: Sm

Deleted: Ssu

Deleted: Si

Deleted: Slo

Deleted: none scheme

Deleted: ,

Deleted: compared to the bulk scheme, the snwITDrdg scheme leads to increased snow-ice formation.

Deleted: particles

Deleted: scheme

precipitation, resulting in reduced overall snow accumulation. Meanwhile, the snwITDrdgm configuration increases snow loss into leads relative to snwITDrdg, thereby reducing snowmelt at the end of the simulation. The sublimation losses are relatively consistent across all snow redistribution schemes. Prescribing sea ice concentration has minimal effect on the no-redistribution experiment and bulk schemes. However, within the snwITDrdg and snwITDrdgm scheme, prescribing sea ice concentration leads to a significant reduction in snow loss into leads and a corresponding increase in snowmelt. This difference arises because the bulk redistribution scheme primarily reduces incoming snowfall through a prescribed level-ice-dependent fraction, making it less sensitive to changes in sea ice concentration. In contrast, the snwITDrdg scheme redistributes wind-eroded snow into open leads, so its snow-loss term depends more directly on the open-water fraction. Prescribing AMSR2 sea ice concentration therefore modifies the amount of snow lost to leads and changes the remaining snow available for subsequent melt.

Deleted: scheme

Deleted: Slo

Deleted: Ssu values

Deleted: none

Deleted: Slo

Deleted: Sm

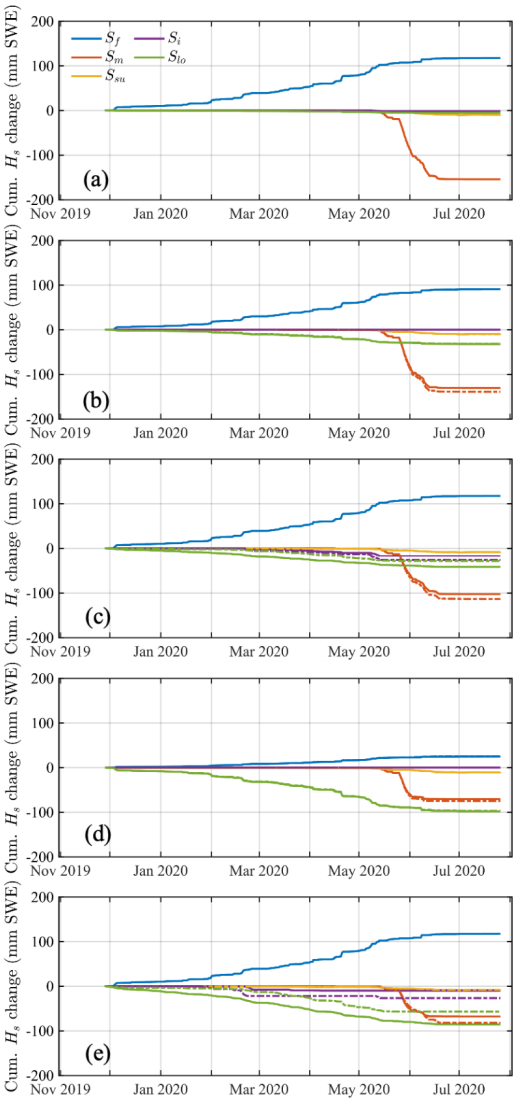


Figure 4. Time series of cumulative snow depth changes in (a) no-redistribution, (b) bulk, (c) snwITDrdg, (d) bulkm and (e) snwITDrdgm redistribution configurations. Different colored lines represent snowfall (S_f), snowmelt (S_m), snow sublimation (S_{su}), snow-ice formation (S_i), and snow loss into open leads (S_{lo}), respectively. Solid lines denote simulations without prescribed AMSR2 sea ice concentration, while dashed

Deleted: none
Deleted: schemes
Deleted: Sf
Deleted: Sm
Deleted: Ssu
Deleted: Si
Deleted: Slo

lines indicate simulations with prescribed AMSR2 sea ice concentration.

4. Conclusions

Snow plays a vital role in sea ice thermodynamics, yet snow accumulation remains a key uncertainty in sea ice modeling. Using the Icepack column model, we simulated snow thickness during the MOSAiC campaign under two snow redistribution parameterizations and multiple model configurations, and further explored both bulk and blowing snow redistribution parameterizations to enhance the agreement with observations. Our results show that without snow redistribution, simulated snow thickness is significantly overestimated in winter and spring. The bulk redistribution scheme slightly reduces snow accumulation, but does not substantially change the timing of the seasonal peak or melt onset. The snwITDrdg redistribution scheme further reduces snow thickness and improves the magnitude of the simulated seasonal evolution, though biases persist, especially during snowfall events and around the seasonal peak.

To address this issue, we conducted sensitivity experiments for both snow redistribution schemes. In the bulk scheme, we varied the parameter p from 0.3 to 4 based on MOSAiC observations. When p = 4, the simulated snow thickness shows the best agreement with observations, with a mean absolute error (MAE) of 6.2 mm. In the snwITDrdg scheme, given the large observational uncertainties in snow density and subgrid-scale ice thickness distribution (ITD), the coefficient γ is treated as an effective tuning parameter that accounts for unresolved uncertainties in snow physical properties and ice thickness heterogeneity. We varied γ from 1×10^{-5} to 3×10^{-5}, with and without prescribing AMSR2 sea ice concentration. When sea ice concentration is not prescribed, adjusting γ does not lead to accumulated snow loss to leads within the observed range of 7-11 mm area-averaged SWE. In contrast, when AMSR2 sea ice concentration is prescribed, the simulated accumulated snow loss to leads falls within

Deleted: and Discussions

Deleted: under various snow redistribution schemes

Deleted: snwITDrdg parameterization

Deleted: , resulting in a delayed seasonal peak and an earlier snow melt in summer

Deleted:

Deleted: while showing a modest improvement in seasonal timing…

Deleted: P

Deleted: P

Deleted: γ

Deleted: γ

Deleted: γ

Deleted: per lead area

the observed range. Specifically, when γ = 2.4×10^{-5}, the simulated snow thickness generally agrees well with observations, yielding a mean absolute error of 6.4 mm. These results indicate that the parameter p in the bulk scheme and the effective tuning coefficient γ in the snwITDrdg scheme both have a significant influence on simulated snow thickness. Moreover, accurate sea ice concentration is crucial for realistic snow thickness simulations in the snwITDrdg scheme.

5. Discussions

Despite improvements in the optimized bulk redistribution and blowing-snow redistribution configurations, several limitations remain. The simulated snow thickness still peaks approximately seven days later than observed and melts too quickly in summer. This discrepancy may partly stem from uncertainties in snowfall forcing. Wagner et al. (2022) showed that MOSAiC snowfall estimates differ among products, and we used the PWD–ERA5 average to reduce product-dependent uncertainty. However, event-scale biases in snowfall timing, frequency, or magnitude may remain. For example, between May 6 and 13, the PWD–ERA5 average shows increased snowfall (Figure 1c), whereas the observed snow thickness declined. We interpret this mismatch as a possible overestimate of snowfall during this event. However, this discrepancy may also reflect unresolved snow-loss processes, including sublimation of drifting and blowing snow, non-local snow transport, and limitations in the model representation of snow compaction and density evolution. Rapid summer melt may also result from missing melt-pond physics or inaccurate snow thermal conductivity, leading to excessive surface heat fluxes (Yin et al., 2021). In addition, Icepack estimates a constant snow density of 330 kg m^{-3}, whereas actual snow density evolves with wind compaction, temperature fluctuations, moisture content, and sublimation (Liston et al., 2020; Macfarlane et al., 2023), contributing to mass and thickness biases. The treatment of suspended snow particles is simplified in Icepack: the fraction of suspended snow that is passed directly to the ocean through leads. While sublimation of suspended snow

Formatted: Font: (Default) Times New Roman Bold, Bold

Formatted: List Paragraph, Level 1, Numbered + Level: 1 + Numbering Style: 1, 2, 3, … + Start at: 1 + Alignment: Left + Aligned at: 0 cm + Indent at: 0 cm

Formatted: Normal, No bullets or numbering

Deleted: Despite improvements, several limitations remain.

Deleted: This discrepancy likely stems from uncertainties in snowfall datasets. For example, the PWD–ERA5 average shows increased snowfall between May 6 and 13 (Figure 1c), while observed snow thickness declined, suggesting potential errors in observations or reanalysis (Wagner et al., 2022).

Deleted: all excess snow is assumed to enter leads

represents an important loss pathway in the Arctic (Liston et al., 2020, Robinson et al. 2025), it is not explicitly represented in the present model configuration. As a result, the optimized p and γ values should be interpreted as effective parameters that may compensate for multiple unresolved snow-loss processes, including lead trapping, wind-driven redistribution, and blowing-snow sublimation, as well as possible biases in snowfall forcing.

Deleted: the distinction between atmospheric and oceanic loss pathways does not affect the results of this study.

Previous studies have shown that snow accumulation and redistribution vary among different sea-ice regimes because of differences in ice age, ice type, deformation state, and surface roughness (Clemens-Sewall et al., 2022). Field observations have also demonstrated pronounced subgrid-scale spatial variability in snow thickness (Huang et al., 2026; Mallett et al., 2022). However, Icepack assumes a spatially uniform snow thickness within each ice-thickness category and therefore does not explicitly resolve this subgrid-scale heterogeneity, which may introduce uncertainty into the simulated snow distribution and its thermodynamic influence on sea ice. Consequently, the parameter p and the performance of snow redistribution parameterizations may vary under different sea-ice conditions. The observational dataset used in this study includes both first-year ice and second-year ice conditions. However, the limited number of available SIMBA buoy sites does not allow a robust evaluation of individual parameterization schemes for specific ice regimes or subgrid-scale snow variability. Therefore, the evaluation presented here is based on the mean snow thickness over the observational region, and the optimized parameter values and conclusions should be interpreted as representing the average snow redistribution behaviour across the range of sea-ice conditions sampled during MOSAiC. Since the same model assumption is adopted consistently in all simulations, it is unlikely to affect the relative comparison among the snow redistribution parameterizations examined in this study. Future work incorporating more realistic representations of subgrid-scale snow heterogeneity together with expanded observational datasets will help further quantify these uncertainties and improve the representation of snow redistribution processes under

different sea-ice conditions.

Our study is complementary to Zhao et al. (2025), who evaluated Icepack simulations along the MOSAiC drift trajectory using no-redistribution, bulk redistribution, and snwITDrdg configurations. Zhao et al. (2025) focused mainly on sea ice thickness and the combined influence of snow redistribution and melt-pond schemes. In contrast, the present study focuses on snow thickness/SWE and the snow mass budget, especially the sensitivity of simulated snow loss to leads to the bulk redistribution parameter p, the blowing-snow erosion coefficient γ, and prescribed AMSR2 sea ice concentration. Therefore, while both studies show that snow redistribution strongly affects Icepack simulations during MOSAiC, our analysis provides a more direct evaluation of snow redistribution parameterizations against MOSAiC snow observations and observed lead-related snow loss. Differences between the results of the two studies likely arise from differences in forcing data, model version and configuration, sea ice concentration treatment, observational constraints, and the specific target variable used for evaluation.

Deleted: ¶
Previous studies have shown that snow accumulation and redistribution vary among different sea-ice regimes because of differences in ice age, ice type, deformation state, and surface roughness (Clemens-Sewall et al., 2022). Therefore, the parameter P and the performance of snow redistribution parameterizations may also vary under different sea-ice conditions. The observational dataset used in this study includes both FYI and SYI conditions. However, the limited number of available SIMBA buoy sites does not allow a robust evaluation of individual schemes for specific ice regimes. Consequently, the optimized parameter values and the conclusions presented here should be interpreted as representing the average snow redistribution behaviour across the range of sea-ice conditions sampled during MOSAiC rather than universally applicable values. Future studies with expanded observational datasets are needed to quantify how snow redistribution processes and model performance depend on ice age, ice type, deformation, and surface roughness.

Although the representativeness of the MOSAiC observations should be considered, they constitute one of the most comprehensive datasets for examining snow and sea ice processes in the central Arctic. The findings of this study provide new insights into snow thickness simulation and the parameterization of snow redistribution, contributing to improved modeling of Arctic snow conditions.

Data availability

The MOSAiC meteorological data are available from the Arctic Data Center (Cox et al., 2021a, 2021b, 2021c, 2023). SIMBA ice and snow thickness data are available from PANGAEA (Lei et al., 2021). Autonomous sea ice measurements (Ocean CTD Buoy and Flux Buoy) from 1 October 2019 to 1 September 2020 were obtained from the

Alfred Wegener Institute Sea Ice Portal (Grosfeld et al., 2016). AMSR2 ASI sea ice concentration data were obtained from the University of Bremen Sea Ice Portal (Melsheimer and Spreen, 2019) and are calculated following Spreen et al. (2008). SAR-based sea ice divergence data drift during MOSAiC 2019/2020 are available from PANGAEA (von Albedyll, 2024).

Deleted: Sea Ice Portal

Competing interests

At least one of the (co-)authors is a member of the editorial board of The Cryosphere

Author contributions

JL, CL and FG conceptualized this study and designed the numerical experiments. FG carried out the numerical experiments and wrote the manuscript. CL, BH, QY and JL helped analyze the results and revised the manuscript.

Acknowledgments

The authors would like to thank all persons involved in the international Multidisciplinary drifting Observatory for the Study of Arctic Climate (MOSAiC) expedition. We acknowledge the University of Colorado/NOAA surface flux team for the effort in collecting and post-processing the meteorological measurements. We appreciate the Polar Research Institute of China for the efforts in obtaining ice thickness and snow thickness data from the SIMBA buoys. The buoy data from 1 October 2019 to 1 September 2020 were obtained from https://www.meereisportal.de (funding: REKLIM-2013-04). AMSR2 ASI sea ice concentration data were provided by the Institute of Environmental Physics, University of Bremen. We are grateful to CICE Consortium for sharing Icepack and its documentation (https:// github.com/CICE-Consortium/Icepack).

Financial support

This research is supported by the National Key R&D Program of China (2022YFE0106300), the National Natural Science Foundation of China (42506245).

References

Bitz, C. M.: Description of initial conditions and forcing data for the SHEBA single column model runs, University of Washington, available at: https://atmos.washington.edu/~bitz/column_model/notes_forcing_data (last access: 16 January 2026).

Bliss, A. C., Hutchings, J. K., and Watkins, D. M.: Sea ice drift tracks from autonomous buoys in the MOSAiC Distributed Network, Scientific Data, 10, 403, https://doi.org/10.1038/s41597-023-02311-y, 2023.

Callaghan, T. V., Johansson, M., Brown, R. D., Groisman, P. Ya., Labba, N., Radionov, V., Barry, R. G., Bulygina, O. N., Essery, R. L. H., Frolov, D. M., Golubev, V. N., Grenfell, T. C., Petrushina, M. N., Razuvaev, V. N., Robinson, D. A., Romanov, P., Shindell, D., Shmakin, A. B., Sokratov, S. A., Warren, S., and Yang, D.: The Changing Face of Arctic Snow Cover: A Synthesis of Observed and Projected Changes, AMBIO, 40, 17-31, https://doi.org/10.1007/s13280-011-0212-y, 2011.

Cheng, B., Launiainen, J., and Vihma, T.: Modelling of Superimposed Ice Formation and SubSurface Melting in the Baltic Sea, Geophysica, 39, 31-50, 2003.

Chung, Y.-C., Bélair, S., and Mailhot, J.: Blowing snow on Arctic sea ice: Results from an improved sea ice-snow-blowing snow coupled system, Journal of Hydrometeorology, 12, 678–689, https://doi.org/10.1175/2011JHM1293.1, 2011.

Clemens-Sewall, D., Polashenski, C., Frey, M. M., Cox, C. J., Granskog, M. A., Macfarlane, A. R., Fons, S. W., Schmale, J., Hutchings, J. K., von Albedyll, L., Arndt, S., Schneebeli, M., and Perovich, D.: Snow Loss Into Leads in Arctic Sea Ice: Minimal in Typical Wintertime Conditions, but High During a Warm and Windy Snowfall Event, Geophysical Research Letters, 50, e2023GL102816, https://doi.org/10.1029/2023GL102816, 2023.

867 Clemens-Sewall, D., Smith, M. M., Holland, M. M., Polashenski, C., and Perovich, D.: Snow redistribution onto
868 young sea ice: Observations and implications for climate models, Elementa: Science of the Anthropocene, 10, 00115,
869 https://doi.org/10.1525/elementa.2021.00115, 2022.

870 Cox, C., Gallagher, M., Shupe, M., Persson, O., Blomquist, B., Grachev, A., Riihimaki, L., Kutchenreiter, M., Morris,
871 V., Solomon, A., Brooks, I., Costa, D., Gottas, D., Hutchings, J., Osborn, J., Morris, S., Preusser, A., and Uttal, T.:
872 Met City meteorological and surface flux measurements (Level 3 Final), Multidisciplinary Drifting Observatory for
873 the Study of Arctic Climate (MOSAiC), central Arctic, October 2019-September 2020, Arctic Data Center,
874 https://doi.org/10.18739/A2PV6B83F, 2023.

875 Cox, C., Gallagher, M., Shupe, M., Persson, O., Solomon, A., Ayers, T., Costa, D., Hutchings, J., Leach, J., Morris,
876 S., Osborn, J., Pezoa, S., and Uttal, T.: Atmospheric Surface Flux Station #30 measurements (Level 1 Raw),
877 Multidisciplinary Drifting Observatory for the Study of Arctic Climate (MOSAiC), central Arctic, October 2019-
878 September 2020, Arctic Data Center, https://doi.org/10.18739/A20C4SM1J, 2021a.

879 Cox, C., Gallagher, M., Shupe, M., Persson, O., Solomon, A., Ayers, T., Costa, D., Hutchings, J., Leach, J., Morris,
880 S., Osborn, J., Pezoa, S., and Uttal, T.: Atmospheric Surface Flux Station #40 measurements (Level 1 Raw),
881 Multidisciplinary Drifting Observatory for the Study of Arctic Climate (MOSAiC), central Arctic, October 2019-
882 September 2020, Arctic Data Center, https://doi.org/10.18739/A2CJ87M7G, 2021b.

883 Cox, C., Gallagher, M., Shupe, M., Persson, O., Solomon, A., Ayers, T., Costa, D., Hutchings, J., Leach, J., Morris,
884 S., Osborn, J., Pezoa, S., and Uttal, T.: Atmospheric Surface Flux Station #50 measurements (Level 1 Raw),
885 Multidisciplinary Drifting Observatory for the Study of Arctic Climate (MOSAiC), central Arctic, October 2019-
886 September 2020, Arctic Data Center, https://doi.org/10.18739/A2445HD46, 2021c.

887 Déry, S. J., and Yau, M. K.: Large-scale mass balance effects of blowing snow and surface sublimation, Journal of
888 Geophysical Research: Atmospheres, 107, ACL 8-1-ACL 8-17, https://doi.org/10.1029/2001JD001251, 2002.

889 Déry, S. J. and Tremblay, L. B.: Modeling the effects of wind redistribution on the snow mass budget of polar sea
890 ice, Journal of Physical Oceanography, 34, 258–271, https://doi.org/10.1175/1520-

0485(2004)034<0258:MTEOWR>2.0.CO;2, 2004.

Eicken, H., Grenfell, T. C., Perovich, D. K., Richter-Menge, J. A., and Frey, K.: Hydraulic controls of summer Arctic pack ice albedo, Journal of Geophysical Research: Oceans, 109, https://doi.org/10.1029/2003JC001989, 2004.

Granskog, M. A., Rösel, A., Dodd, P. A., Divine, D., Gerland, S., Martma, T., and Leng, M. J.: Snow contribution to first-year and second-year Arctic sea ice mass balance north of Svalbard, Journal of Geophysical Research: Oceans, 122, 2539-2549, https://doi.org/10.1002/2016JC012398, 2017.

Grosfeld, K., Treffeisen, R., Asseng, J., Bartsch, A., Bräuer, B., Fritzsch, B., Gerdes, R., Hendricks, S., Hiller, W., Heygster, G., Krumpen, T., Lemke, P., Melsheimer, C., Nicolaus, M., Ricker, R., and Weigelt, M.: Online sea-ice knowledge and data platform, Polarforschung, 85, 143 − 155, https://doi.org/10.2312/polfor.2016.011, 2016.

Gu, F., Kauker, F., Yang, Q., Han, B., Fang, Y., and Liu, C.: Effects of Freezing Temperature Parameterization on Simulated Sea-Ice Thickness Validated by MOSAiC Observations, Geophysical Research Letters, 51, e2024GL108281, https://doi.org/10.1029/2024GL108281, 2024.

Gu, F., Yang, Q., Kauker, F., Liu, C., Hao, G., Yang, C.-Y., Liu, J., Heil, P., Li, X., and Han, B.: The sensitivity of landfast sea ice to atmospheric forcing in single-column model simulations: a case study at Zhongshan Station, Antarctica, The Cryosphere, 16, 1873 − 1887, https://doi.org/10.5194/tc-16-1873-2022, 2022.

Hao, G., Shen, H., and Sun, Y.: Simulation and analysis of the snow blowing on landfast sea ice, Antarctica, Acta Oceanologica Sinica, 44, 161-171, https://doi.org/10.1007/s13131-025-2464-6, 2025.

Huang, L., Stroeve, J., Newman, T., Mallett, R., Willatt, R., Zhou, L., Johansson, M., Nab, C., and Fallows, A.: Snow depth distributions on sea ice of different ages and thicknesses from regional field campaigns, The Cryosphere, 20, 2825–2849, https://doi.org/10.5194/tc-20-2825-2026, 2026.

Hunke, E., Allard, R., Bailey, D. A., Blain, P., Craig, T., Dupont, F., DuVivier, A., Grumbine, R., Hebert, D., Holland, M., Jeffery, N., Lemieux, J.-F., Rasmussen, T., Ribergaard, M., and Roberts, A.: CICE-Consortium/Icepack: Icepack

913 1.3.2, Zenodo, https://doi.org/10.5281/zenodo.6967671, 2022.

914 Itkin, P., Hendricks, S., Webster, M., von Albedyll, L., Arndt, S., Divine, D., Jaggi, M., Oggier, M., Raphael, I.,
915 Ricker, R., Rohde, J., Schneebeli, M., and Liston, G. E.: Sea ice and snow characteristics from year-long transects
916 at the MOSAiC Central Observatory, Elementa: Science of the Anthropocene, 11, 00048,
917 https://doi.org/10.1525/elementa.2022.00048, 2023.

918 Jeffries, M. O., Krouse, H. R., Hurst-Cushing, B., and Maksym, T.: Snow-ice accretion and snow-cover depletion
919 on Antarctic first-year sea-ice floes, Annals of Glaciology, 33, 51-60, https://doi.org/10.3189/172756401781818266,
920 2001.

921 Kwok, R.: Arctic sea ice thickness, volume, and multiyear ice coverage: losses and coupled variability (1958-2018),
922 Environmental Research Letters, 13, 105005, https://doi.org/10.1088/1748-9326/aae3ec, 2018.

923 Lecomte, O., Fichefet, T., Flocco, D., Schroeder, D., and Vancoppenolle, M.: Interactions between wind-blown snow
924 redistribution and melt ponds in a coupled ocean-sea ice model, Ocean Modelling, 87, 67-80,
925 https://doi.org/10.1016/j.ocemod.2014.12.003, 2015.

926 Lecomte, O., Fichefet, T., Vancoppenolle, M., Domine, F., Massonnet, F., Mathiot, P., Morin, S., and Barriat, P. Y.:
927 On the formulation of snow thermal conductivity in large-scale sea ice models, Journal of Advances in Modeling
928 Earth Systems, 5, 542-557, https://doi.org/10.1002/jame.20039, 2013.

929 Lei, R., Cheng, B., and Hoppmann, M.: Snow depth and sea ice thickness derived from the measurements of SIMBA
930 buoys deployed in the Arctic Ocean during the Legs 1a, 1, and 3 of the MOSAiC campaign in 2019-2020,
931 PANGAEA, https://doi.org/10.1594/PANGAEA.938244, 2021.

932 Lei, R., Cheng, B., Heil, P., Vihma, T., Wang, J., Ji, Q., and Zhang, Z.: Seasonal and interannual variations of sea
933 ice mass balance from the Central Arctic to the Greenland Sea, Journal of Geophysical Research: Oceans, 123, 2422-
934 2439, https://doi.org/10.1002/2017JC013548, 2018.

935 Lei, R., Cheng, B., Hoppmann, M., Zhang, F., Zuo, G., Hutchings, J. K., Lin, L., Lan, M., Wang, H., Regnery, J.,

936 Krumpen, T., Haapala, J., Rabe, B., Perovich, D. K., and Nicolaus, M.: Seasonality and timing of sea ice mass
937 balance and heat fluxes in the Arctic transpolar drift during 2019 – 2020, Elementa: Science of the Anthropocene,
938 10, 000089, https://doi.org/10.1525/elementa.2021.000089, 2022.

939 Leonard, K. C., and Maksym, T.: The importance of wind-blown snow redistribution to snow accumulation on
940 Bellingshausen Sea ice, Annals of Glaciology, 52, 271-278, https://doi.org/10.3189/172756411795931651, 2011.

941 Leppäranta, M.: A Growth Model for Black Ice, Snow Ice and Snow Thickness in Subarctic Basins, Hydrology
942 Research, 14, 59-70, https://doi.org/10.2166/nh.1983.0006, 1983.

943 Liston, G. E., Itkin, P., Stroeve, J., Tschudi, M., Stewart, J. S., Pedersen, S. H., Reinking, A. K., and Elder, K.: A
944 Lagrangian Snow-Evolution System for Sea-Ice Applications (SnowModel-LG): Part I—Model Description, Journal
945 of Geophysical Research: Oceans, 125, e2019JC015913, https://doi.org/10.1029/2019JC015913, 2020.

946 Luo, L., and Zhang, J.: Blowing Snow Contributes to Positive Surface Energy Budget and Negative Surface Mass
947 Balance During a Melting Season of Larsen C Ice Shelf, Antarctic Peninsula, Geophysical Research Letters, 49,
948 e2022GL098864, https://doi.org/10.1029/2022GL098864, 2022.

949 Macfarlane, A., Schneebeli, M., Dadic, R., Tavri, A., Immerz, A., Polashenski, C., Krampe, D., Clemens-Sewall, D.,
950 Wagner, D., Perovich, D., Hannula, H.-R., Raphael, I., Matero, I., Regnery, J., Smith, M., Nicolaus, M., Jaggi, M.,
951 Oggier, M., Webster, M., and Fons, S.: A Database of Snow on Sea Ice in the Central Arctic Collected during the
952 MOSAiC expedition, Scientific Data, 10, https://doi.org/10.1038/s41597-023-02273-1, 2023.

953 Maksym, T., and Jeffries, M. O.: A one-dimensional percolation model of flooding and snow ice formation on
954 Antarctic sea ice, Journal of Geophysical Research: Oceans, 105, 26313-26331,
955 https://doi.org/10.1029/2000JC900130, 2000.

956 Mallett, R. D. C., Stroeve, J. C., Tsamados, M., Willatt, R., Newman, T., Nandan, V., Landy, J. C., Itkin, P., Oggier,
957 M., Jaggi, M., and Perovich, D.: Sub-kilometre scale distribution of snow depth on Arctic sea ice from Soviet drifting
958 stations, Journal of Glaciology, 68, 1014–1026, https://doi.org/10.1017/jog.2022.18, 2022.

Massom, R. A., Eicken, H., Hass, C., Jeffries, M. O., Drinkwater, M. R., Sturm, M., Worby, A. P., Wu, X., Lytle, V. I., Ushio, S., Morris, K., Reid, P. A., Warren, S. G., and Allison, I.: Snow on Antarctic sea ice, Reviews of Geophysics, 39, 413 – 445, https://doi.org/10.1029/2000RG000085, 2001.

Maykut, G. A., and Untersteiner, N.: Some results from a time-dependent thermodynamic model of sea ice, Journal of Geophysical Research, 76, 1550-1575, https://doi.org/10.1029/JC076i006p01550, 1971.

Melsheimer, C. and Spreen, G.: AMSR2 ASI sea ice concentration data, Arctic, version 5.4 (NetCDF), PANGAEA, https://doi.org/10.1594/PANGAEA.898399, 2019.

Merkouriadi, I., Cheng, B., Graham, R. M., Rösel, A., and Granskog, M. A.: Critical Role of Snow on Sea Ice Growth in the Atlantic Sector of the Arctic Ocean, Geophysical Research Letters, 44, 10479-10485, https://doi.org/10.1002/2017GL075494, 2017.

Merkouriadi, I., Liston, G. E., Graham, R. M., and Granskog, M. A.: Quantifying the Potential for Snow-Ice Formation in the Arctic Ocean, Geophysical Research Letters, 47, e2019GL085020, https://doi.org/10.1029/2019GL085020, 2020.

Merkouriadi, I., Jutila, A., Liston, G. E., Preußer, A., and Webster, M. A.: Investigating snow sinks on level sea ice: A case study in the western Arctic, Journal of Glaciology, 71, e66, https://doi.org/10.1017/jog.2025.34, 2025.

Perovich, D. K., Grenfell, T. C., Light, B., and Hobbs, P. V.: Seasonal evolution of the albedo of multiyear Arctic sea ice, Journal of Geophysical Research: Oceans, 107, SHE 20-1-SHE 20-13, https://doi.org/10.1029/2000JC000438, 2002.

Perovich, D., Raphael, I., Moore, R., Clemens-Sewall, D., Lei, R., Sledd, A., and Polashenski, C.: Sea ice heat and mass balance measurements from four autonomous buoys during the MOSAiC drift campaign, Elementa: Science of the Anthropocene, 11, 00017, https://doi.org/10.1525/elementa.2023.00017, 2023.

Petty, A. A., Webster, M., Boisvert, L., and Markus, T.: The NASA Eulerian Snow on Sea Ice Model (NESOSIM) v1.0: initial model development and analysis, Geoscientific Model Development, 11, 4577-4602,

https://doi.org/10.5194/gmd-11-4577-2018, 2018.

Polashenski, C., Perovich, D., and Courville, Z.: The mechanisms of sea ice melt pond formation and evolution, Journal of Geophysical Research: Oceans, 117, 2011JC007231, https://doi.org/10.1029/2011JC007231, 2012.

Rabe, B., Heuzé, C., Regnery, J., Aksenov, Y., Allerholt, J., Athanase, M., Bai, Y., Basque, C., Bauch, D., Baumann, T. M., Chen, D., Cole, S. T., Craw, L., Davies, A., Damm, E., Dethloff, K., Divine, D. V., Doglioni, F., Ebert, F., Fang, Y.-C., Fer, I., Fong, A. A., Gradinger, R., Granskog, M. A., Graupner, R., Haas, C., He, H., He, Y., Hoppmann, M., Janout, M., Kadko, D., Kanzow, T., Karam, S., Kawaguchi, Y., Koenig, Z., Kong, B., Krishfield, R. A., Krumpen, T., Kuhlmey, D., Kuznetsov, I., Lan, M., Laukert, G., Lei, R., Li, T., Torres-Valdés, S., Lin, L., Lin, L., Liu, H., Liu, N., Loose, B., Ma, X., McKay, R., Mallet, M., Mallett, R. D. C., Maslowski, W., Mertens, C., Mohrholz, V., Muilwijk, M., Nicolaus, M., O'Brien, J. K., Perovich, D., Ren, J., Rex, M., Ribeiro, N., Rinke, A., Schaffer, J., Schuffenhauer, I., Schulz, K., Shupe, M. D., Shaw, W., Sokolov, V., Sommerfeld, A., Spreen, G., Stanton, T., Stephens, M., Su, J., Sukhikh, N., Sundfjord, A., Thomisch, K., Tippenhauer, S., Toole, J. M., Vredenborg, M., Walter, M., Wang, H., Wang, L., Wang, Y., Wendisch, M., Zhao, J., Zhou, M., and Zhu, J.: Overview of the MOSAiC expedition: Physical oceanography, Elementa: Science of the Anthropocene, 10, 00062, https://doi.org/10.1525/elementa.2021.00062, 2022.

Robinson, J., Jaeglé, L., Palm, S. P., Shupe, M. D., Liston, G. E., and Frey, M. M.: ICESat-2 observations of blowing snow over Arctic sea ice during the 2019–2020 MOSAiC expedition, Journal of Geophysical Research: Atmospheres, 130, e2025JD043919, https://doi.org/10.1029/2025JD043919, 2025.

Robinson, J., Jaeglé, L., Palm, S. P., and Liston, G. E.: Blowing snow contributions to the Arctic snow-on-sea ice budget using ICESat-2 observations, The Cryosphere, 20, 3217–3233, https://doi.org/10.5194/tc-20-3217-2026, 2026.

Ruti, P. M., Marullo, S., D'Ortenzio, F., and Tremant, M.: Comparison of analyzed and measured wind speeds in the perspective of oceanic simulations over the Mediterranean basin: Analyses, QuikSCAT and buoy data, Journal of Marine Systems, 70, 33-48, https://doi.org/10.1016/j.jmarsys.2007.02.026, 2008.

1006 Salganik, E., Lange, B. A., Itkin, P., Divine, D., Katlein, C., Nicolaus, M., Hoppmann, M., Neckel, N., Ricker, R.,
1007 Høyland, K. V., and Granskog, M. A.: Different mechanisms of Arctic first-year sea-ice ridge consolidation observed
1008 during the MOSAiC expedition, Elementa: Science of the Anthropocene, 11, 00008,
1009 https://doi.org/10.1525/elementa.2023.00008, 2023.

1010 Schmidt, R. A.: Vertical profiles of wind speed, snow concentration, and humidity in blowing snow, Boundary-
1011 Layer Meteorology, 23, 223-246, https://doi.org/10.1007/BF00123299, 1982.

1012 Shupe, M. D., Rex, M., Blomquist, B., Persson, P. O. G., Schmale, J., Uttal, T., Althausen, D., Angot, H., Archer,
1013 S., Bariteau, L., Beck, I., Bilberry, J., Bucci, S., Buck, C., Boyer, M., Brasseur, Z., Brooks, I. M., Calmer, R., Cassano,
1014 J., Castro, V., Chu, D., Costa, D., Cox, C. J., Creamean, J., Crewell, S., Dahlke, S., Damm, E., de Boer, G.,
1015 Deckelmann, H., Dethloff, K., Dütsch, M., Ebell, K., Ehrlich, A., Ellis, J., Engelmann, R., Fong, A. A., Frey, M. M.,
1016 Gallagher, M. R., Ganzeveld, L., Gradinger, R., Graeser, J., Greenamyer, V., Griesche, H., Griffiths, S., Hamilton,
1017 J., Heinemann, G., Helmig, D., Herber, A., Heuzé, C., Hofer, J., Houchens, T., Howard, D., Inoue, J., Jacobi, H.-W.,
1018 Jaiser, R., Jokinen, T., Jourdan, O., Jozef, G., King, W., Kirchgaessner, A., Klingebiel, M., Krassovski, M., Krumpen,
1019 T., Lampert, A., Landing, W., Laurila, T., Lawrence, D., Lonardi, M., Loose, B., Lüpkes, C., Maahn, M., Macke,
1020 A., Maslowski, W., Marsay, C., Maturilli, M., Mech, M., Morris, S., Moser, M., Nicolaus, M., Ortega, P., Osborn,
1021 J., Pätzold, F., Perovich, D. K., Petäjä, T., Pilz, C., Pirazzini, R., Posman, K., Powers, H., Pratt, K. A., Preußer, A.,
1022 Quéléver, L., Radenz, M., Rabe, B., Rinke, A., Sachs, T., Schulz, A., Siebert, H., Silva, T., Solomon, A., et al.:
1023 Overview of the MOSAiC expedition: Atmosphere, Elementa: Science of the Anthropocene, 10, 00060,
1024 https://doi.org/10.1525/elementa.2021.00060, 2022.

1025 Spreen, G., Kaleschke, L., and Heygster, G.: Sea ice remote sensing using AMSR-E 89-GHz channels, Journal of
1026 Geophysical Research: Oceans, 113, https://doi.org/10.1029/2005JC003384, 2008.

1027 Sturm, M., Holmgren, J., and Perovich, D. K.: Winter snow cover on the sea ice of the Arctic Ocean at the Surface
1028 Heat Budget of the Arctic Ocean (SHEBA): Temporal evolution and spatial variability, Journal of Geophysical
1029 Research: Oceans, 107, SHE 23-1-SHE 23-17, https://doi.org/10.1029/2000JC000400, 2002.

Van den Broeke, M. R., Reijmer, C. H., and Van De Wal, R. S.: A study of the surface mass balance in Dronning Maud Land, Antarctica, using automatic weather stations, Journal of Glaciology, 50, 565-582, https://doi.org/10.3189/172756504781829756, 2004.

von Albedyll, L.: Sea ice lead fractions from SAR-derived sea ice divergence in the Transpolar Drift during MOSAiC 2019/2020 [Dataset], PANGAEA, https://doi.org/10.1594/PANGAEA.963671, 2024.

Wagner, D. N., Shupe, M. D., Cox, C., Persson, O. G., Uttal, T., Frey, M. M., Kirchgaessner, A., Schneebeli, M., Jaggi, M., Macfarlane, A. R., Itkin, P., Arndt, S., Hendricks, S., Krampe, D., Nicolaus, M., Ricker, R., Regnery, J., Kolabutin, N., Shimanshuck, E., Oggier, M., Raphael, I., Stroeve, J., and Lehning, M.: Snowfall and snow accumulation during the MOSAiC winter and spring seasons, The Cryosphere, 16, 2373 – 2402, https://doi.org/10.5194/tc-16-2373-2022, 2022.

Wang, C., Cheng, B., Wang, K., Gerland, S., and Pavlova, O.: Modelling snow ice and superimposed ice on landfast sea ice in Kongsfjorden, Svalbard, Polar Research, 34, 20828, https://doi.org/10.3402/polar.v34.20828, 2015.

Webster, M., Gerland, S., Holland, M., Hunke, E., Kwok, R., Lecomte, O., Massom, R., Perovich, D., and Sturm, M.: Snow in the changing sea-ice systems, Nature Clim Change, 8, 946 – 953, https://doi.org/10.1038/s41558-018-0286-7, 2018.

Yin, H., Su, J., and Cheng, B.: The effect of snow density evolution on modelled snow depth in the Arctic, Haiyang Xuebao, 43, 15, 2021.

Zhao, J., Lu, Y., Zhao, H., Wang, X., and Liu, J.: Influence of Snow Redistribution and Melt Pond Schemes on Simulated Sea Ice Thickness During the MOSAiC Expedition, Journal of Marine Science and Engineering, 13, 1317, https://doi.org/10.3390/jmse13071317, 2025.

1052